EFFECTS OF BEARING DEADBANDS ON BEARING LOADS AND ROTOR STABILITY

John R. Glaese and Angelia P. Bukley
Control Dynamics Company
Huntsville, Alabama 35805

Introduction

The problem of determining bearing loads and stability properties of rotating machines such as the turbopumps used in high performance rocket engines like the Space Shuttle Main Engine (SSME) is complex. Very high speeds are attained with significant fluid flows. As a consequence, bearing loads are potentially high with subsynchronous whirling likely. Typically, models used to analyze such systems are very complicated and nearly impossible to use for gaining insight into the basic phenomena involved. Linear models containing large numbers of degrees of freedom have been developed and applied to the analysis with mixed success. A significant nonlinearity is ignored by these models. The bearings typically have clearances of the order of .0005"-.0025". Since these machines are balanced to very high precision, the eccentricity of the rotor, i.e. the distance between the rotor center of mass and its geometric axis is of the same order or smaller in magnitude. Thus, bearing clearances or deadbands as they are more typically called, significantly affect the dynamics of these systems and must be taken into account. Taking this nonlinearity into account makes the analysis of the dynamics much more difficult. It is very desirable to have a simplified model of a turbopump which retains the significant driving forces known to be present but readily lends itself to analysis. Such a model is available and is usually referred to as the Jeffcott model. We have modified this model by adding deadband effects along with fluid seal forces as currently understood. Further, we have rewritten the equations of motion for the model in

polar coordinates. This formulation is more naturally suited to the symmetry of the problem because the whirl orbits tend to be circular.

In addition to seal forces and deadbands, we have added a constant side force to the model to account for the likely misalignments between bearings and seals and also to account for hydrodynamic forces resulting from pumping fluids which may not be perfectly balanced due to slight imperfections in the internal geometry of the pump. The side force and deadband effects, working together, significantly affect the stability properties of the system in an interesting way. Stability may be enhanced under proper combinations but is only local stability in that it is possible to drive the system into instability by impulsive disturbances or large rotor imbalances.

The Jeffcott rotor is closer to reality than it may appear to the casual observer. Periodic synchronous or nonsynchronous orbiting motions of the rotor, referred to as whirls, are normally the motions of the system exhibited. Such an orbital motion can be described by a planar model. Thus, values for the effective mass, stiffness, deadband and seal coefficients can be found which will approximate the behavior of the more complex models. While exact frequencies of critical speeds and stability boundaries cannot be inferred from Jeffcott models, very good qualitative behavior can be investigated with these models and refined by higher fidelity hybrid simulations. For this reason, we consider the augmented Jeffcott model as the model of choice for developing an understanding of rotor whirl phenomena.

Force Models & System Equations of Motion

The assumed geometry for the derivation of the equations of motion of the simple rotor model is depicted in Figure 1. The vector r is the displacement of the rotor center from its equilibrium position (rotor at rest). The angle ϕ is the angle made by r with the horizontal axis and is referred to as
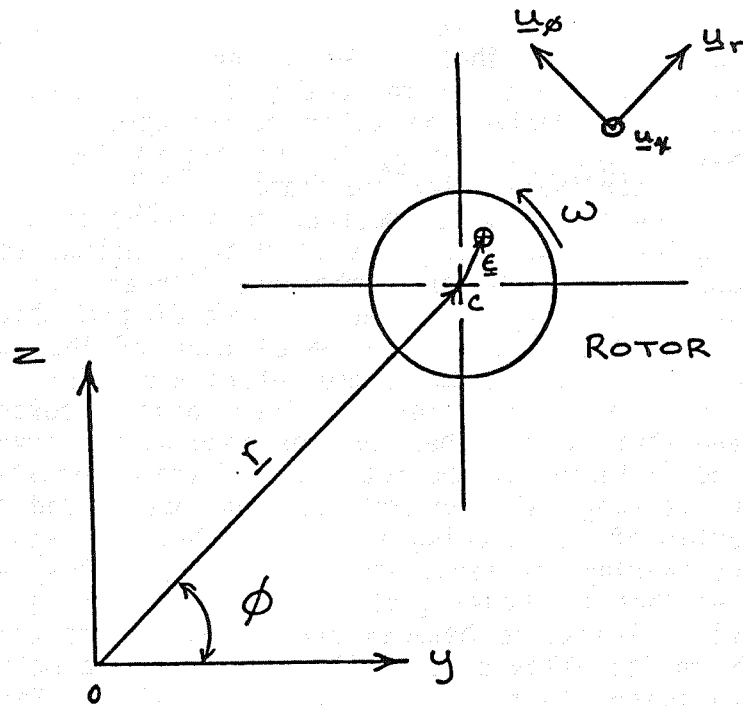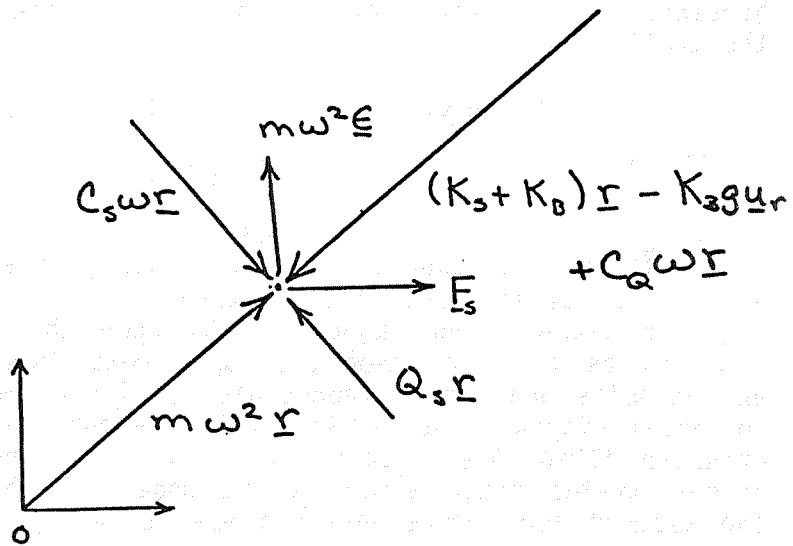
Figure 1. Assumed rotor geometry.

Figure 2. Vector force diagram.

the whirl angle. The rotor eccentricity is repre-
sented by the vector ε, the magnitude of which is
constant. The shaft speed is denoted by ω and is
assumed constant for the analysis. The equations of
motion are derived in polar coordinates. The unit
vectors $\underline{u}_r$, $\underline{u}_\phi$, and $\underline{u}_x$ in the figure indicate the
polar coordinate reference frame.

The forces which must be considered in the for-
mulation of the equations of motion include bearing
forces, seal forces, imbalance forces, and side
forces. Figure 2 is a vector force diagram which in-
dicates the direction in which each of the various
forces acts. The turbopump rotors are maintained in
position by bearing forces. These bearing forces are
generated by a rather complex interaction involving
bending forces of the rotor shaft, the deformation of
the bearing balls or rollers, the motion and defor-
mation of the bearing races, the bearing retainers,
the bearing carriers, etc. For our purposes, we as-
sume that the bearing acts as a linear spring. How-
ever, clearances between bearing races and carriers
or shafts allow some small region of free motion of
the rotor shaft relative to its housing. For sim-
plicity, we idealize the bearing balls or rollers as
a uniform annular ring separating the rotor shaft and
housing. The bearing force curve is idealized for
the analysis as

$$\underline{F}_B = \begin{cases} K_B \ (\underline{r} - g \ \underline{u}_r) & |\underline{r}| > g \\ 0 & |\underline{r}| \le g \end{cases} \tag{1}$$

where K_B is the bearing stiffness and g is the dead-
band. If the magnitude of r is less than g, then the
bearing forces are assumed to be zero.

The fluid being pumped reacts upon the rotor
with forces that are dependent upon rotor position
and velocity and can be represented by linear models
for small displacements.[1] The seals prevent the high
pressure fluid from leaking away and also generate
forces on the rotor which can be modeled linearly.
The assumed form representing these forces is given
by

$$\underline{F}_{seal} = -C_s \dot{\underline{r}} - K_s \underline{r} + Q_s \underline{u}_x \times \underline{r} + C_Q \underline{u}_x \times \dot{\underline{r}} \qquad (2)$$

where K_s is the seal stiffness, C_s is the seal damping coefficient, Q_s is the cross coupling stiffness, and C_Q is the cross coupling damping. These forces have the potential to drive whirl instability.

The force due to the mass eccentricity is a rotating force whose magnitude varies as the square of the rotor speed and is directed toward the rotor center of mass. This force is potentially destructive and must be minimized by stringent balancing of the turbopump rotors. The form of this force is

$$\underline{F}_e = -m \omega^2 \underline{\varepsilon} \qquad (3)$$

with m representing the mass of the rotor. The values of the parameters in the equations above are chosen such that the system model is representative of the SSME high-pressure oxygen turbopump. These values are: $K_B = 10^6$ lbs/in; $K_S = 2.0 \times 10^5$ lbs/in; $C_S = 200$ lbs-sec/in; $C_Q = 40$ lbs-sec/in; $Q_S = C_S\omega/2$ lbs/in; and $m = 0.20422$ lbs-sec^2/in. Five deadband values are considered and are 0.5, 1.0, 1.5, 2.0, and 2.5 mils. Two values of rotor eccentricity are also used, they are 0.1 and 0.2 mils. Side force values range from 600 to 1200 pounds in the investigation.

The force equation for the system may be written as

$$m(\ddot{\underline{r}} + \ddot{\underline{\varepsilon}}) = \sum_i \underline{F}_i \quad , \qquad (4)$$

with the summation representing the forces due to the seals, bearings, and the side force. The vector equation for the system is, therefore

$$m\ddot{\underline{r}} = -K_B (\underline{r} - g\underline{u}_r) - K_s \underline{r} - C_s \dot{\underline{r}} +$$

$$Q_s \underline{u}_x \times \underline{r} + C_Q \underline{u}_x \times \dot{\underline{r}} + \underline{F}_s + m \omega^2 \underline{\varepsilon}. \qquad (5)$$

Performing the vector cross products and derivatives indicated in equation 5 above, the following second

order differential equations which describe the system are obtained.

$$\ddot{r} = \frac{-K_B}{m}(r-g) - \frac{K_S}{m}r - \frac{C_S}{m}\dot{r} - \frac{C_Q}{m}r\dot{\phi} + \frac{F_S}{m}\cos\phi +$$

$$r\dot{\phi}^2 + \omega^2\epsilon\cos(\omega t - \phi) \qquad (6)$$

$$\ddot{\phi} = \frac{Q_S}{m} - \frac{C_S}{m}\dot{\phi} + \frac{C_Q}{m}\frac{\dot{r}}{r} - \frac{F_S}{m}\sin\phi - \frac{2r\dot{\phi}}{r}$$

$$(7)$$

$$+ \frac{\omega^2\epsilon}{r}\sin \quad (\omega t - \phi)$$

Limit Cycle Analysis

Analysis of the system is more readily carried out when the equations of motion are cast in state variable form.

Let

$$p_1 = r \qquad p_2 = \dot{r} \qquad p_3 = \phi \qquad p_4 = \dot{\phi} \qquad (8)$$

Then

$$\dot{p}_1 = p_2 \qquad (9)$$

$$\dot{p}_2 = \frac{-(K_B + K_S)}{m}p_1 + K_B g - \frac{C_S}{m}p_2 - \frac{C_Q}{m}p_1 p_4$$

$$(10)$$

$$+ \frac{F_S}{m}\cos p_3 + \omega^2\epsilon\cos(\omega t - p_3) + p_1 + p_4^2$$

$$\dot{p}_3 = p_4 \qquad (11)$$

$$\dot{p}_4 = \frac{Q_s}{m} - \frac{C_s}{m} p_4 + \frac{C_Q\, p_2}{m\, p_1} - \frac{F_s}{m\, p_1} \sin p_3$$

$$+ \frac{\omega^2 \epsilon}{p_1} \sin(\omega t - p_3) - \frac{2\, p_2 p_4}{p_1} \tag{12}$$

In this form, the system is amenable to solution by numerical methods. Three different types of orbits are observed when the system of equation is solved for different values of deadband, side force, and rotor eccentricity. These are referred to as A-type, B-type, and C-type motion.[2] Illustrations of the three are shown in Figures 3 through 5. A-type motion is periodic and does not encircle the origin. B-type motion is nonperiodic and somewhat random in nature. C-type is periodic and does surround the origin. The A-type and C-type motions are limit cycles.

To characterize the limit cycle motions present in the rotor system, an algorithm has been developed which will converge to a set of initial conditions for the four system states which, when input into a simulation of this system, will cause the system to immediately exhibit the limit cycle behavior. The algorithm is based on the fact that the function for which the limit cycle initial conditions are sought is periodic. That is, the orbit comes back around to the same point once each cycle. The idea is to determine that such a point exists and the values of the system states which satisfy this condition.

Given the state equations which describe the system, a solution to the states may be obtained through integration. The mathematical statement of the problem is:

$$\underline{\dot{p}} = \underline{f}(\underline{p}, t) \tag{13}$$
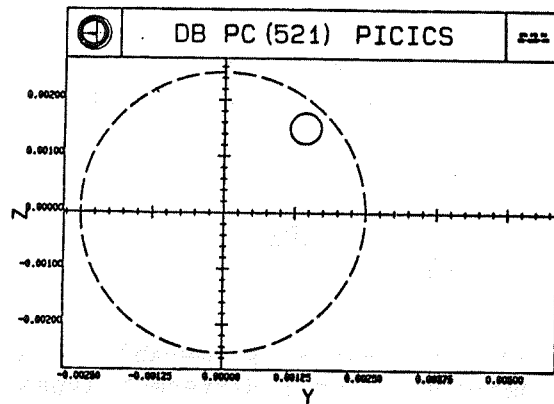
the solution to which is

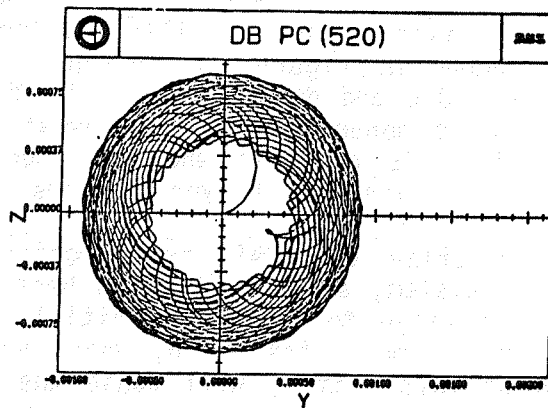Figure 3. A-type rotor motion.

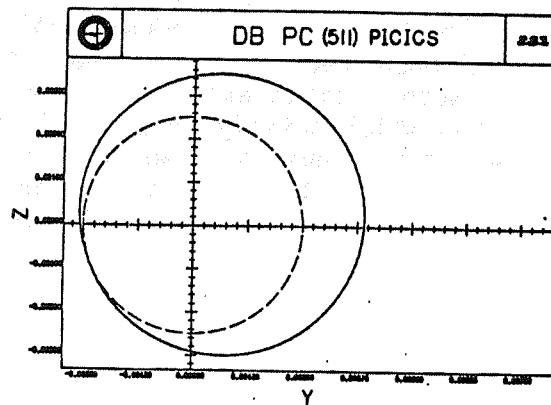

Figure 4. B-type rotor motion.

Figure 5. C-type rotor motion.

352

$$\underline{p}(t) = \underline{p}_0 + \int_0^t \underline{f}(\underline{p}, \tau) d\tau \tag{14}$$

where $\underline{p}_0$ is some initial state. It is desired to determine the $\underline{p}_0$ such that

$$\underline{p}(t) = \underline{p}_0 \quad \text{for } t = T \tag{15}$$

$$\text{where } T = \frac{2\pi}{\omega}, \tag{16}$$

the period of the function. In other words, we wish to determine $\underline{p}_0$ so that the integral in Equation 14 is zero. The problem may be restated as

$$\underline{p}(T) = \underline{p}_0 + \underline{g}(\underline{p}) . \tag{17}$$

If $\underline{g}(\underline{p})$ can be driven to zero, then $\underline{p}(T) = \underline{p}_0$.

The function $\underline{g}(\underline{p})$ may be approximated to 1st order by

$$\underline{g}(\underline{p}) = \underline{g}(\underline{p}_0) + \left. \frac{\partial \underline{g}}{\partial \underline{p}} \right|_{\underline{p}_0} \cdot \Delta \underline{p} \tag{18}$$

where $\Delta \underline{p}$ is some incremental change in the state vector $\underline{p}$. This is the quantity to be determined. It will be added to the original state vector. Because we wish $\underline{g}(\underline{p})$ to be zero, Equation 17 is rewritten as

$$\underline{0} = \underline{g}(\underline{p}_0) + \underline{\underline{J}} \cdot (\underline{p} - \underline{p}_0) \tag{19}$$

where

$$\Delta \underline{p} = \underline{p} - \underline{p}_0 \tag{20}$$

and $\underline{\underline{J}}$ is the Jacobian of $\underline{g}(\underline{p})$. The solution for $\Delta \underline{p}$ is

$$\Delta \underline{p} = \underline{\underline{J}}^{-1} \left(-\underline{g}(p_0) \right) . \tag{21}$$

A new set of initial states is formed as

$$\underline{p}_{0_{new}} = \underline{p}_{0_{old}} + \Delta \underline{p} . \tag{22}$$

For orbits which are C-type, another modification to the algorithm is required. Because the whirl angle, ϕ, is not periodic but increasing with time, this method left unmodified will not converge to a solution. To force ϕ to appear to be periodic, the value 2π is subtracted from the ϕ component of the state vector value at time $t = T$. This procedure will, in fact, allow the algorithm to converge to a solution to the C-type orbit initial conditions.

The plot of the limit cycle shown in Figure 3 is obtained using the initial conditions obtained with the algorithm described above. Figure 6 is a plot of that same limit cycle including the transients that occur when a simulation of the system is executed with the initial conditions set at zero. Likewise, the plot in Figure 5 is obtained using limit cycle initial conditions obtained with the algorithm. Figure 7 is a plot of the same orbit obtained from zero initial conditions.

Stability Analysis

The approach taken in the determination of system stability is to examine the equations of motion, omitting the imbalance force terms. This procedure greatly simplifies the analysis. Our studies indicate that side forces and deadbands are influential on local stability. Under the influence of a side force, the rotor shifts to a position of equilibrium when no imbalance is present. The addition of an imbalance, in general, causes the rotor to whirl about the equilibrium point. The position of the equilibrium point is dependent upon the magnitude of the side force, the deadband, and the stiffness coefficients. The position of the equilibrium, with respect to the deadband, determines the type of orbit
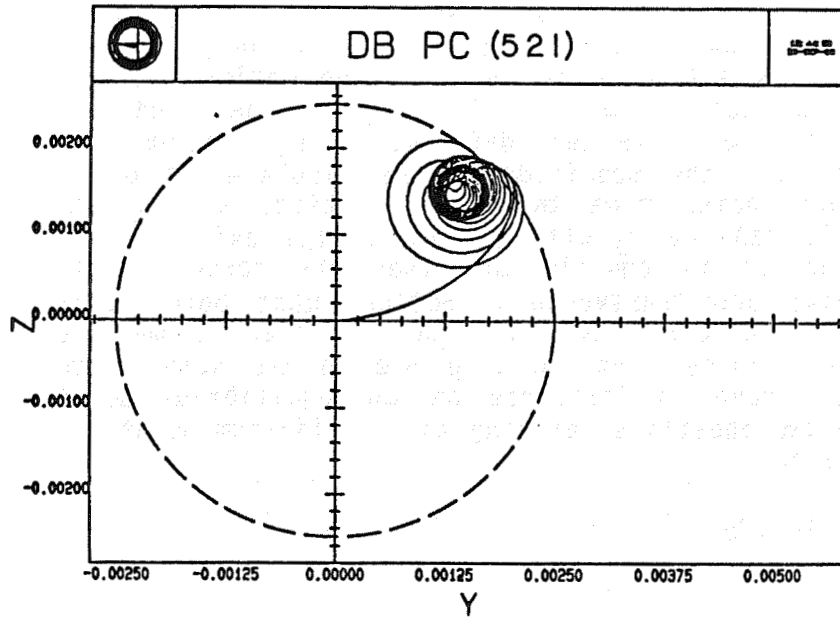
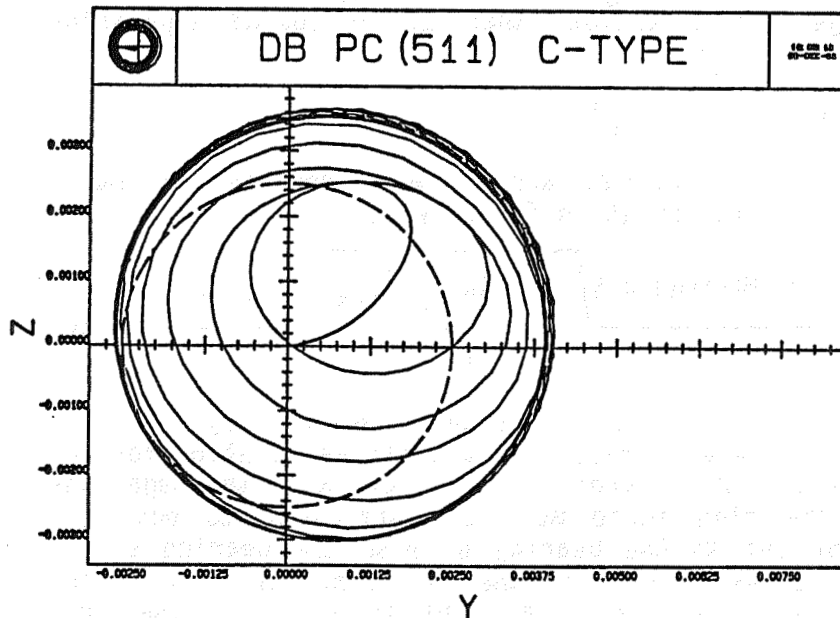Figure 6. A-type motion with transients.

Figure 7. C-type motion with transients.

in which the rotor will whirl. Generally, if the equilibrium point is outside the deadband, the rotor exhibits A-type motion with C-type motion resulting if the equilibrium point is inside the deadband.

The two parameters defining the equilibrium point are r_0, the magnitude of the displacement of the rotor center from the rest position, and ϕ_0, the angle made by r_0 with the horizontal axis. If the rotor is in equilibrium, then the forces in the radial and transverse directions must both sum to zero. Because they have been balanced by the side force, force terms arising due to the spin of the shaft have no influence on the equilibrium point. The two equations defining the equilibrium point are, therefore,

$$K_B (r_0 - g) + K_S r_0 = F_S \cos \phi_0 \qquad (23)$$

$$Q_S r_0 = F_S \sin \phi_0 \qquad (24)$$

where F_S is used to denote side force magnitude. If we define F_r to be the side force in the radial direction and F_ϕ to be the side force in the tangential direction, then the following expression is true.

$$F_S^2 = F_r^2 + F_\phi^2 \qquad (25)$$

Using equations 23 and 24 with equation 25 makes possible the solution for r_0 which is

$$r_0 = \frac{(K_B+K_S)K_B g \pm \sqrt{F_S^2[(K_B+K_S)^2+Q_S^2] - Q_S^2 K_B^2 g^2}}{(K_B + K_S)^2 + Q_S^2} \qquad (26)$$

Note that when there is no deadband, any value of side force will result in a positive solution for r_0. However, in the presence of a deadband, the magnitude of the side force must be sufficient to push the rotor out to the bearing or else the bearing stiffness plays no role in the determination of r_0. The minimum side force required to overcome the seal

stiffness is denoted F_{SMIN} and is defined by the expression

$$F_{SMIN} = \sqrt{(K_s{}^2 + Q_s{}^2)g^2} \; .$$
(27)

For any value of side force less than F_{SMIN}, the value of r_0 is the positive solution to Equation 26 with K_B set to zero. For cases in which the side force is greater than F_{SMIN} and two positive solutions result, then r_0 is equal to the larger of the two values because it will lie outside the deadband due to the side force being sufficient to move the rotor to such a position. The angle ϕ_0 is easily obtained once the solution for r_0 is determined.

With the equilibrium points well in hand, we may now proceed. Recall the vector equation which describes the system. It is repeated here, with the imbalance term omitted.

$$m\ddot{\underline{r}} = -K_B(r - g) \; u \; (r - g) \; \underline{e}_r - K_s r \underline{e}_r + Q_s \underline{e}_x \times r\underline{e}_r$$

$$- C_s \dot{\underline{r}} + C_Q \underline{e}_x \times \dot{\underline{r}}$$
(28)

We make the following definitions for $\underline{r}$ and $\underline{e}_r$,

$$\underline{r} = \underline{r}_0 + \underline{\delta}$$
(29)

$$r = r_0 + \delta_y$$
(30)

$$\underline{e}_r = \underline{e}_{r_0} + \delta\underline{e}_r$$
(31)

where r_0 is the equilibrium position vector, $\underline{e}_{r_0}$ is the unit vector in the direction of $\underline{r}_0$, and $\underline{\delta}$ and $\delta\underline{e}r$ are the perturbations associated with $\underline{r}$ and $\underline{e}_r$, respectively. The radial component of $\underline{r}$ with its perturbation is Equation 30. Another way to express $\underline{e}_r$ is

$$\underline{e}_r = \frac{\underline{r}_0 + \underline{\delta}}{|\underline{r}_0 + \underline{\delta}|} = \frac{\underline{r}_0}{|\underline{r}_0|} + \frac{\underline{\delta}}{|\underline{r}_0|} - \frac{\underline{r}_0 \, \underline{r}_0}{|r_0|^2} \cdot \underline{\delta}$$

$$+ \ldots$$
(32)

which is equivalent to:

$$\underline{e}_r = \underline{e}_{r_0} + \frac{\delta z}{r_0} \underline{e}_\phi \quad . \tag{33}$$

We now examine the nonlinear deadband term in Equation 27. In the small and to a first order approximation,

$$-K_B (r - g) u (r - g) \underline{e}_r$$

$$= -K_B r_0 \underline{e}_{ro} + K_B g \underline{e}_{r_0} - K_B \delta y \underline{e}_{r_0} - K_B \frac{(r_0 - g)}{r_0} \delta z \underline{e}_\phi \tag{34}$$

with δy and δz being the small perturbations about the equilibrium. It follows, therefore, that in terms of the perturbation variables, the system may be expressed in the following form:

$$m \begin{bmatrix} \ddot{\delta} y \\ \ddot{\delta} z \end{bmatrix} = - \begin{bmatrix} K_S + K_B & Q \\ -Q & K_S + K_B (1 - g_0) \end{bmatrix} \begin{bmatrix} \delta y \\ \delta z \end{bmatrix}$$

$$- \begin{bmatrix} C_S & C_Q \\ -C_Q & C_S \end{bmatrix} \begin{bmatrix} \dot{\delta} y \\ \dot{\delta} z \end{bmatrix} \quad . \tag{35}$$

Where $g_0 = \dfrac{g}{r_0}$.

The effects of side forces are now inherent in the formulation. Stability may be assessed through examination of equation 35. State assignments for the perturbation variables are given below.

$$x_1 = \delta_y \qquad x_2 = \dot{\delta}_y \qquad x_3 = \delta_z \qquad x_4 = \dot{\delta}_z \quad (36)$$

Rewriting 34 in state variable format yields the following differential equations.

$$\dot{x}_1 = x_2 \tag{37}$$

$$\dot{x}_2 = -\frac{K}{m} x_1 - \frac{C_S}{m} x_2 - \frac{Q_S}{m} x_3 - \frac{C_Q}{m} x_4 \tag{38}$$

$$\dot{x}_3 = x_4 \tag{39}$$

$$\dot{x}_4 = \frac{Q_S}{m} x_1 + \frac{C_Q}{m} x_2 - \frac{K_S + K_B (1 - g_0)}{m} x_3 \tag{40}$$

$$-\frac{C_S}{m} x_4$$

The sum $K_B + K_S$ has been replaced by K for simplicity's sake. The system matrix is formed as before from which the characteristic equation is derived by solving the determinant of $[sI - A]$.

$$P(s) = \left[s^2 + \frac{C_S}{m} s + K + \Delta^2 - \frac{Q_S^2}{m^2} \right]$$

$$\left[s^2 + \frac{C_S}{m} s + K - \Delta^2 - \frac{Q_S^2}{m^2} \right]$$

$$\tag{41}$$

The stability boundaries established are plotted in Figure 8. Several interesting facts are observed when this figure is examined. The stability boundary for a deadband of zero is a constant 4848 radians/second, the dashed curve in the figure. This is the same stability boundary which may be established for the simplest form of the system.[3] This frequency is considered to be the global stability boundary. That
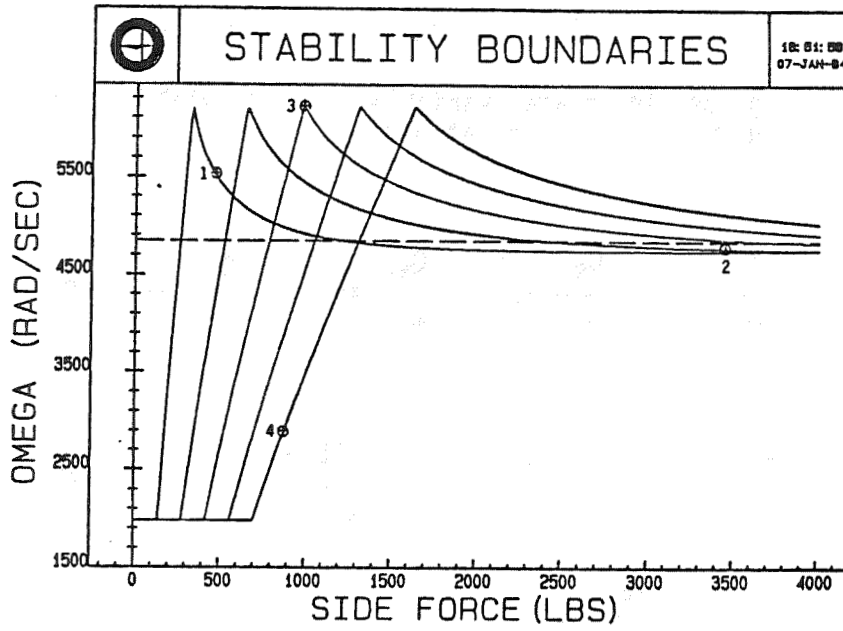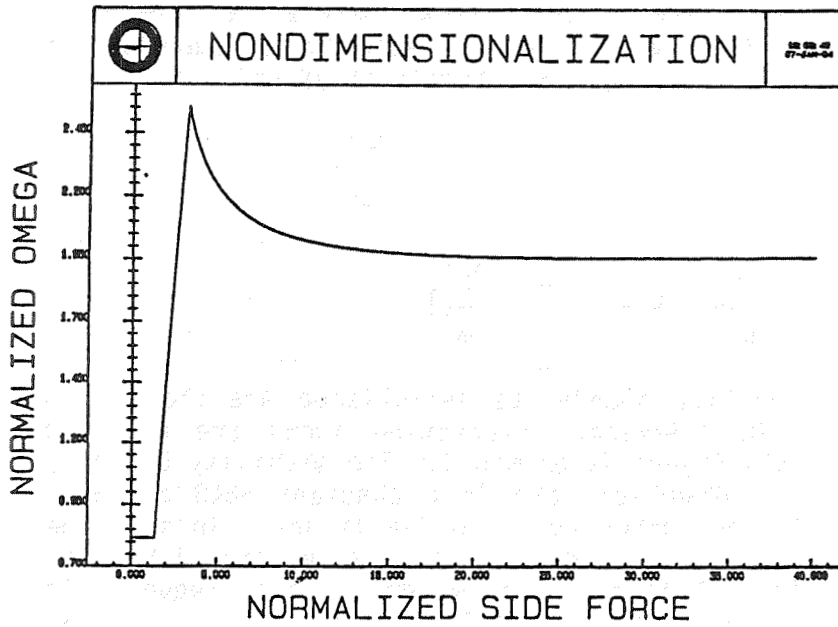
Figure 8.   Stability boundaries.

Figure 9.   Nondimensionalized stability boundary.

is, the system is globally unstable when run at frequencies higher than this value. Local stability, or stability in the small, may be enhanced by other factors.

Notice that all five of the non-zero deadband stability curves are very similar in their general character. The maxima appear at approximately the same spin frequency as do their minima. We have shown that these curves do, indeed, collapse into a single curve when the system is nondimensionalized. To accomplish this, the units of displacement, force, and time are modified in such a way that the system parameters become unitless. Displacements are expressed in units of g, the deadband. Forces may be expressed as the product of the seal stiffness and deadband. Time is expressed in terms of the system natural frequency is $\sqrt{m/(K_s + K_B)}$. Figure 9 is a plot of the stability boundary for the normalized system. With this curve and the given conversion factors, one may determine the stability boundary for any deadband value.

Bearing Loads Considerations

One of the major points of the study is to determine the effects of the system parameters on bearing loads. If these loads become too large, the effects are detrimental. Initially, we will look into this matter using a system with no side forces present, but with a rotor imbalance. We will then take into consideration the added effects of a side force present in the system.

Plotted in Figure 10 are the bearing loads which result when the rotor eccentricity is 0.1 mils. The deadband range is from 0.0 to 0.2 mils. The general behavior is that the smaller deadband produces the largest bearing load. This makes sense because the seal forces must be overcome before there is any interaction between the rotor and the bearings. The more distance between the rotor and the bearing there is, the more effect the seal forces have. It has been shown that if the rotor eccentricity is doubled, the bearing loads also double if all other parameters are left unchanged.[3]
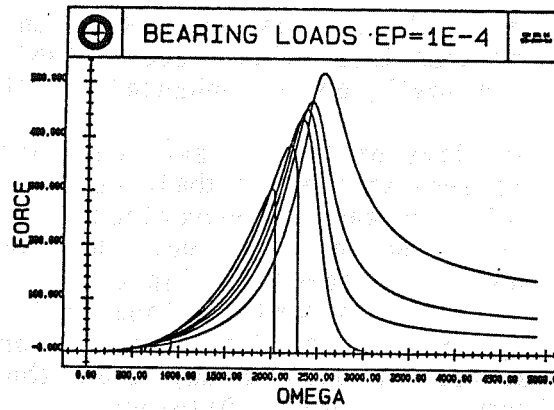
361

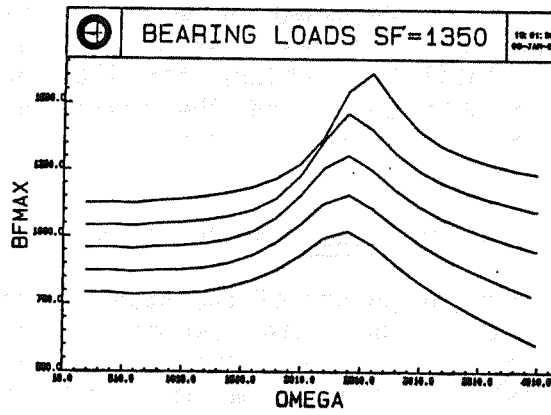Figure 10. Bearing force curves.

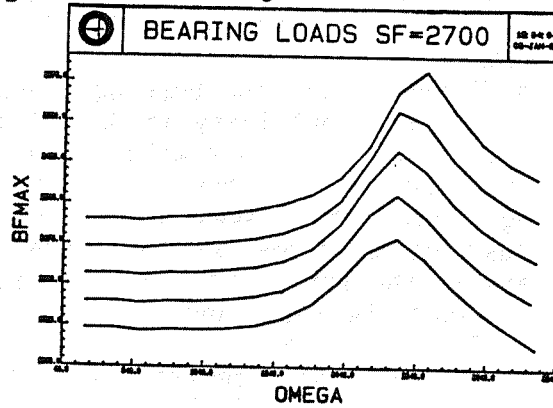Figure 11. Bearing force curves.

Figure 12. Bearing force curves.

Bearing load analysis is performed for two non-zero side force values. A value of side force is chosen so that it is always greater than F_{SMIN} for any of the five deadbands considered up to a frequency of 5000 radians per second. Figure 11 is a plot of the bearing loads for the deadbands of 0.5 to 2.5 mils for the side force of 1350 pounds. The maximum bearing loads occur at the system natural frequency of approximately 2424 radians/second, the smallest deadband producing the largest load. The load curves are plotted only up to a shaft spin frequency of 4000 radians because the system becomes unstable for frequencies higher than that. The presence of the rotor eccentricity of 0.2 mils is responsible for the unstable behavior.

A similar family of curves is produced when the side force is increased to twice that of the "minimum" side force, or, 2700 pounds. The plots of these bearing loads are given in Figure 12. The same general behavior is exhibited as before. Instability occurs somewhat sooner, at 3400 radians/second. The loads are much greater, as well.

The curves presented were generated using the simulation to determine the maximum rotor displacement, after steady-state is achieved. Having this value, it is a simple matter to compute the bearing load. Equation 43 is used.

$$BF_{MAX} = K_B(r_{MAX} - g) \tag{43}$$

Conclusions

In the previous sections we have discussed the modeling and analysis of the problem. It is now time to review and summarize our results.
1. Observed 3 motion types called A, B, C;
    A - Periodic but does not enclose origin, may include higher harmonics;
    B - Nonperiodic;
    C - Periodic enclosing origin, synchronous or nonsynchronous;

2. Limit Cycle Algorithm developed and employed, both A & C types observed.

3. Deadband does not affect stability-in-the-large.

4. Stability-in-the-small are affected (enhanced) by deadband and sideforce.

5. Bearing loads are largest for C-type motion.

6. Side force acting in concert with deadband effects may either increase or decrease bearing loads.

7. Bearing loads in a stable pump are determined primarily by rotor imbalance and side forces.

These results are quite significant in our understanding of the effects of bearing deadbands. Harmonics of snychronous and nonsynchronous oscillations have been observed. This is clearly a nonlinear effect. Stable limit cycle whirls have been observed occurring at synchronous and nonsynchronous rotor speeds in our results.

The limit cycle algorithm that we have developed can be generalized to more complex turbopump models with more degrees of freedom. It will be useful for loads analysis with nonlinear forces for rotor dynamics and other applications. It is capable of converging to periodic motions (solutions) which generally result in the highest load-producing conditions.

Since stability-in-the-large is ultimately determined by behavior at extremely large amplitudes of motion, deadband effects become negligible. Thus, linear models remain adequate for analysis of global stability properties. Stability-in-the-small is significantly altered by the nonlinear effects of deadbands. We have shown that sideforces can significantly enhance stability provided imbalance offsets and/or impulsive disturbances do not cause significant displacement from the equilibrium position of the rotor.

Bearing loads have been shown to be significantly modified by deadband effects. Critical speeds are altered. Loads may increase or decrease. The shape of the critical response curve is altered with higher loading at lower frequencies due to the deadband.

These results have been obtained using a relatively simple 2 degree-of-freedom model. This may lead one to believe the results are not applicable to real machines. This is not the case, however, and indeed one can argue and demonstrate with more sophisticated models that these effects are real. Since rotor responses are most often periodic, such motions can be described adequately by an effective mass responding to effective stiffnesses and deadbands, i.e., a 2-dimensional model. Thus, our results are at least qualitatively valid for the description of turbo-pump motions.

References

1. Gunter, Edgar J. Jr., Dynamic Stability of Rotor-Bearing Systems, NASA SP-113; 1966.

2. Several G. C. Marshall Space Flight Center, ED14, Internal Memoranda and presentations covering period 1978-1980.

3. Final Report on Contract No. NAS8-35050, "Effects of Bearing Deadbands on Bearing Loads and Rotor Stability", Prepared for G. C. Marshall Space Flight Center by Control Dynamics Company, Huntsville, Alabama, January, 1984.